Optical Society of America. Zhengyu Huang, Yizheng Zhu, and Anbo Wang, "Principles and design of multibeam interference devices: a microelectromechanical-systems segment-deformable-mirror-based adaptive spectrum attenuator," Appl. Opt. 44, 4454-4460 (2005). doi: 10.1364/ao.44.004454

Principles and design of multibeam interference devices: a microelectromechanical-systems segment-deformable-mirror-based adaptive spectrum attenuator

Zhengyu Huang, Yizheng Zhu, and Anbo Wang

Fourier analysis of multibeam interference shows that the total electric field and relative time delay of the beams form a Fourier-transform pair. Fourier-analysis-based multibeam interference analysis and device design is discussed in detail. The principle of the proposed segment-deformable-mirror-based adaptive spectrum attenuator is illustrated. © 2005 Optical Society of America

OCIS codes: 050.2230, 060.4510, 060.4230, 070.2590, 260.3160.

1. Introduction

In wavelength-division multiplexed (WDM) optical communication networks, signals are amplified periodically by erbium-doped fiber amplifiers (EDFAs). Since the gain profile of an EDFA is not flat, attenuators are usually used to maintain signal powers at different wavelengths equal to avoid cross talk and data loss. However, fixed attenuation can only compensate fixed input power and amplification. In an active network, input power and amplifier gain change with time. Active level compensation at each wavelength is needed. An adaptive attenuator is a device with a chromatically variable transmissivity used to equalize channel powers in WDM fiber-optic communication lines.[1] Such a device has been realized by various technologies, such as microelectromechanical systems (MEMS),[2–4] magneto-optic[5] and acousto-optic[6,7] methods, planar lightwave circuits,[8–10] and holograms.[11] In this paper, Fourier analysis of multibeam interference and device design is first presented, followed by the introduction of the proposed segment-deformable-mirror (SDM) based adaptive attenuator.

The authors are with the Center for Photonics Technology, Bradley Department of Electrical and Computer Engineering, Virginia Polytechnic Institute and State University, Blacksburg, Virginia 24061. Z. Huang can be reached by e-mail at zhhuang1@vt.edu.

Received 29 September 2004; revised manuscript received 10 January 2005; accepted 14 January 2005.

0003-6935/05/214454-07$15.00/0

2. Fourier Analysis of Multibeam Interference

A basic understanding of a signal waveform is that it can be decomposed onto and reconstructed by a set of orthogonal basis in the vector space. A Fourier transform is a specification of such an idea. Given a time-domain signal $f(t)$, its Fourier-transform pair is

$$F(\omega) = \mathrm{FT}\{f(t)\} = \int_{-\infty}^{+\infty} f(t)\exp(-j\omega t)\mathrm{d}t,$$

$$f(t) = \mathrm{IFT}\{F(\omega)\} = \frac{1}{2\pi}\int_{-\infty}^{+\infty} F(\omega)\exp(j\omega t)\mathrm{d}\omega, \quad (1)$$

where IFT is inverse Fourier transform.

Fourier transform can also be used in multibeam interference spectrum analysis. Suppose a plane wave of light is incident upon a Fabry–Perot (FP) cavity at an angle θ as shown in Fig. 1, where r and t are the reflection coefficient and the transmission coefficient for a wave traveling from the surrounding medium into the cavity, and r' and t' are the reflection and transmission coefficients for a wave traveling from the cavity to the surrounding medium. The complex magnitude of the transmitted electric field $E^{(t)}$ is

$$E^{(t)}(\omega) = \sum_{p=0}^{\infty} a_p \exp(-jT_p\omega), \quad (2)$$

where $a_p = tt'r'^{2p}E^{(i)}$ is the complex magnitude of the

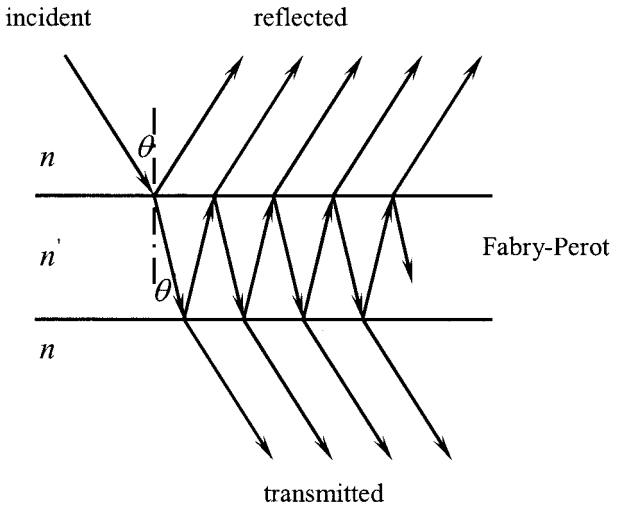

Fig. 1. Fabry–Perot cavity interference model.

pth beam, $E^{(i)}$ is the complex magnitude of the incident light, and $T_p = 2pn'h \cos\theta'/c$ and ωT_p are the relative time delay (RTD) and the relative phase difference, respectively, of the pth beam to the zeroth beam.

$E^{(t)}(\omega)$ is the sum of a Fourier series in Eq. (2). Each component in the Fourier series has a different RTD value and is orthogonal to the others. The components with different RTD values $\{1, \exp(-jT_1\omega), \exp(-jT_2\omega), \exp(-jT_3\omega), \ldots\}$ form a set of orthogonal basis in the RTD domain. Thus, the multibeam interference electric field spectrum $E(\omega)$ can be analyzed in the RTD domain using a Fourier transform. The electric field spectrum $E(\omega)$ and its RTD spectrum $A(T)$ are a Fourier transform pair as shown in Eq. (3):

$$A(T) = \int_{-\infty}^{+\infty} E(\omega)\exp(-jT\omega)\mathrm{d}\omega,$$

$$E(\omega) = \frac{1}{2\pi}\int_{-\infty}^{+\infty} A(T)\exp(jT\omega)\mathrm{d}T. \qquad (3)$$

Consequently, Fourier analysis can be applied to multibeam interference analysis. As we all know for the time-domain signal, the larger the bandwidth, the more the higher frequencies the signal contains, and the more the detail of the signal. Shown in Fig. 2(a) is the RTD amplitude spectrum $|A(T)|$ of three FP cavities with the same optical length but different reflectivity. We can define the bandwidth of the FP cavity as the range of RTD in analogy with that of the time-domain signal. From Fig. 2(a) we know the FP cavity with higher reflectivity has a larger bandwidth, which allows more beams with larger RTD value to participate in the multibeam interference. Thus the electric field spectrum of the FP cavity with higher reflectivity should have more optical spectrum

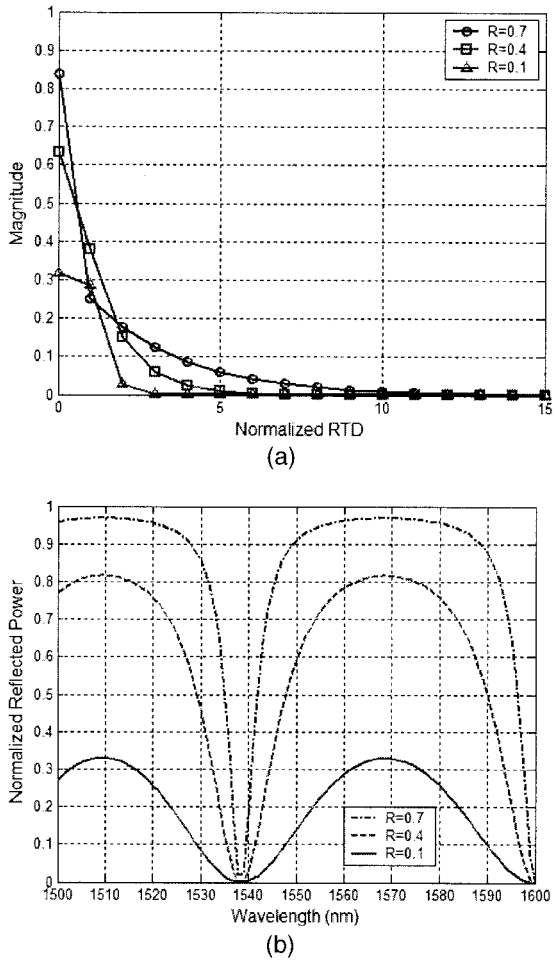

Fig. 2. (a) RTD spectrum $A(T)$ versus different reflectivity for $n = 1$, $h = 20$ μm FP. (b) Reflected spectrum versus different reflectivity for $n = 1$, $h = 20$ μm FP.

detail or fringe contrast than that of the cavity with lower reflectivity, and this is shown in Fig. 2(b).

The concept of RTD bandwidth is important for multibeam interference device. The degree of spectrum detail or sharp contrast that the device can achieve is directly related to its RTD bandwidth. It sets the performance limit of such device. This will provide us a guideline to multibeam interference device design.

3. Multibeam Interference Device Design

Given a target optical intensity spectrum $I(\omega)$, the first step in a multibeam interference device design is to obtain the RTD spectrum $A(T)$ that can be physically realized.

$A(T)$ usually takes the complex form $A(T) = |A(T)|\exp(-j\varphi_T)$. But for a given RTD value T, it is impossible for a device to realize a nonzero constant phase shift φ_T for all the optical wavelengths. Thus for a RTD spectrum $A(T)$ that can be physically realized, $A(T)$ cannot be complex and has to be real. $A(T)$ is obtained from $E(\omega)$ using Eq. (3). According to Eq. (4), the phase spectrum of $E(\omega)$ is lost in $I(\omega)$. $E(\omega)$ with the same magnitude spectrum $|E(\omega)|$ but dif-

ferent phase spectrum $\exp[-j\varphi(\omega)]$ will yield the same $I(\omega)$. The objective becomes to find an $E(\omega) = |E(\omega)|\exp[-j\varphi(\omega)]$ that has a real Fourier transform $A(T)$ and a target intensity spectrum $I(\omega)$:

$$\begin{aligned} I(\omega) &= E(\omega)E^*(\omega) \\ &= |E(\omega)|\exp[-j\varphi(\omega)]\,|E(\omega)|\exp[j\varphi(\omega)] \\ &= |E(\omega)|^2. \end{aligned} \tag{4}$$

The Fourier-transform property shows that a real and even function has a real and even Fourier transform. A real even and imaginary odd function has a real Fourier transform.

Because the phase spectrum of $E(\omega)$ is lost in $I(\omega)$, it is hard to obtain a real even and an imaginary odd $E(\omega)$ from $I(\omega)$. Thus a simple method to generate real $A(T)$ is to obtain real and even $E(\omega)$ from $I(\omega)$. Such $E(\omega)$ forces the real $A(T)$ to be even, which means if an optical beam with RTD value T_i and electric field magnitude $A(T_i)$ participates in the interference, another optical beam with a RTD value of $-T_i$ and an electric field magnitude $A(-T_i)$ must also participate the interference.

The procedure to obtain real and even RTD spectrum $A(T)$ from $I(\omega)$ is broken down into two steps. The first step is to mathematically construct a real and even target electric field spectrum $E_{\text{even}}(\omega)$ using Eq. (5); the second step is to obtain real and even $A(T)$ using Eq. (3):

$$E_{\text{even}}(-\omega) = E_{\text{even}}(\omega) = \sqrt{I_{\text{even}}(\omega)} = \sqrt{I(\omega)},\ \omega \geq 0. \tag{5}$$

The real and even $A(T)$ could contain negative values. In the applications where the bandwidth of interest $[\omega_1, \omega_2]$ is very small compared to the center wavelength ω_c,

$$\frac{\Delta\omega/2}{\omega_c} = \varepsilon \ll 1. \tag{6}$$

Let us define the half-wavelength RTD T_π as

$$T_\pi = \pi/\omega_c. \tag{7}$$

Then the negative $A(T_i) = -|A(T_i)|$ can be realized by introducing a phase shift of π to its absolute value $|A(T_i)|$:

$$\begin{aligned} |A(T_i)|\exp[-j\omega(T_i + T_\pi)] &= -|A(T_i)|\exp(-jT_i\omega) \\ &\quad \times \exp\left(-j\,\frac{\omega-\omega_c}{\omega_c}\,\pi\right) \\ &= A(T_i)\exp(-jT_i\omega) \\ &\quad \times \left[\cos\left(\frac{\omega-\omega_c}{\omega_c}\,\pi\right)\right. \\ &\quad \left. + j\sin\left(\frac{\omega-\omega_c}{\omega_c}\,\pi\right)\right] \\ &\approx A(T_i)\exp(-jT_i\omega). \end{aligned} \tag{8}$$

The term $\cos[\pi(\omega - \omega_c)/\omega_c] + j\sin[\pi(\omega - \omega_c)/\omega_c]$ introduces distortion. The maximum distortion occurs at $\omega = \omega_c \pm \Delta\omega/2$. The distortion is usually very small in real applications and thus can be neglected. For instance, in fiber communication, the erbium-doped fiber amplifiers (EDFAs) have a central wavelength of $\lambda_c = 1550$ nm and an amplify range of $\Delta\lambda = 30$ nm. The maximum distortion is calculated below:

$$\begin{aligned} \cos\left(\frac{\Delta\lambda/2}{\lambda_c - \Delta\lambda/2}\,\pi\right) + j\sin\left(\frac{\Delta\lambda/2}{\lambda_c - \Delta\lambda/2}\,\pi\right) &= 0.9995 \\ &\quad + j0.0307 \approx 1. \end{aligned} \tag{9}$$

The Taylor-series expansion of this distortion term in the vicinity of ω_c is shown in Eq. (10), where distortion can be omitted for very small ε:

$$\begin{aligned} \cos\left(\frac{\omega_c \pm \Delta\omega/2}{\omega_c}\,\pi\right) &= \cos(\pi) + \frac{\cos'(\pi)}{1!}(\pm\varepsilon\pi) \\ &\quad + \frac{\cos''(\pi)}{2!}(\pm\varepsilon\pi)^2 + \ldots \approx 1, \\ \sin\left(\frac{\omega_c \pm \Delta\omega/2}{\omega_c}\,\pi\right) &= \sin(\pi) + \frac{\sin'(\pi)}{1!}(\pm\varepsilon\pi) \\ &\quad + \frac{\cos''(\pi)}{2!}(\pm\varepsilon\pi)^2 + \ldots \approx 0. \end{aligned} \tag{10}$$

The second step in multibeam interference device design is to design a device that can realize the obtained RTD spectrum $A(T)$. To achieve this goal, the device should be able to provide all the RTD components in $A(T)$ and to assign different magnitudes to different RTD components. Once these two conditions are satisfied, the device can reproduce $I(\omega)$ according to Eq. (3).

To assign different magnitudes to different RTD components, the device could be an amplitude-split interferometer that has different reflectivity assigned to different RTD beams, such as optical thin film. The device could also be a wavefront-split interferometer that assign different total reflection areas for different RTD beams, such as the proposed SDM based adaptive attenuator.

To assign all the RTD components in $A(T)$ to the multiple beams, the device should be able to divide the incident wave into multiple beams and then to assign different RTD to different beams. These devices include FP cavity, thin film, fiber Bragg grating, and the proposed SDM based adaptive attenuator.

If one of the two conditions is not satisfied, the optical intensity spectrum will have distortion. The distortion comes from the following sources:

1. The RTD spectrum $A(T)$ has a larger bandwidth than the device. For example, as shown in Fig. 2, the bandwidth of the $R = 0.7$ FP cavity is larger than that of the $R = 0.1$ FP cavity. Thus for a target

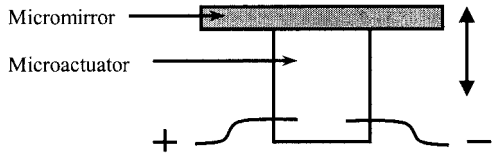

Fig. 3. Basic unit of SDM.

spectrum the same as the $R = 0.7$ FP cavity spectrum, it is inevitable to have spectrum distortion when a $R = 0.1$ FP cavity is used to reproduce it.

2. The device has sufficient bandwidth but fails to provide some RTD components. For example, for a FP cavity with $T_p = 2pn'h \cos\theta'/c$, it can only provide RTDs that are multiples of $2n'h \cos\theta'/c$. If the target spectrum requests an RTD component that is a fraction of T_p, the FP cavity would fail to provide these RTD components and result in distortion.

3. The device is unable to assign the exact magnitude as requested to the beams.

4. Novel Adaptive Attenuator

The reason FP cavities, thin film, and fiber gratings can generate only a fixed shape of a spectrum is because they have fixed RTD components and magnitudes of RTD components assigned to the multiple beams. If to some extent a device can arbitrarily assign these two factors to the beams, the device can generate an arbitrary interference spectrum to a certain extent.

Based on such an idea, we propose a SDM-based adaptive attenuator. A SDM is an array of micromirrors made on a backplane. The vertical position of each mirror can be precisely controlled by an array of microactuators. Figure 3 shows a unit mirror in the SDM. In the following discussion, the SDM parameters of interest are total number of mirrors M, vertical dynamic range L of a unit mirror, and bits of control b. If the SDM has b-bits control, then the resolution of the SDM movement is $L/2^b$, which means the minimum increment of vertical position of a mirror is $L/2^b$.

As shown in Fig. 4(a), a plane wave of light is divided into M beams upon the reflection of each unit mirror in the SDM. The SDM is a wavefront-split interferometer. The RTD assignment among the beams can be illustrated using Fig. 4(b). M_1 and M_2 are two unit mirrors separated by vertical distance $\Delta L = L_1 - L_2$. This would result in phase difference $\delta_{1,2} = 4\pi\Delta L \cos\theta/\lambda$ and RTD $T = 2\Delta L \cos\theta/c$ between the two beams, both of which are linear functions of ΔL. Once we change vertical positions of the reflection mirrors, we can assign RTD among the reflected beams. The RTD component magnitude assignment can be illustrated in Fig. 4(c). M_1, M_2, and M_3 are three unit mirrors. The vertical distances between these mirrors are $\Delta L_{1,2} = 0$, $\Delta L_{1,3} = \Delta L_{2,3} = L_1 - L_3$. Since $\Delta L_{1,2} = 0$, there is no RTD difference between these two beams. Thus they can be regarded as one beam with twice the magnitude of the third beam. Once we change the number of mirrors that have the same RTD value, we can assign RTD component magnitude among the reflected beams.

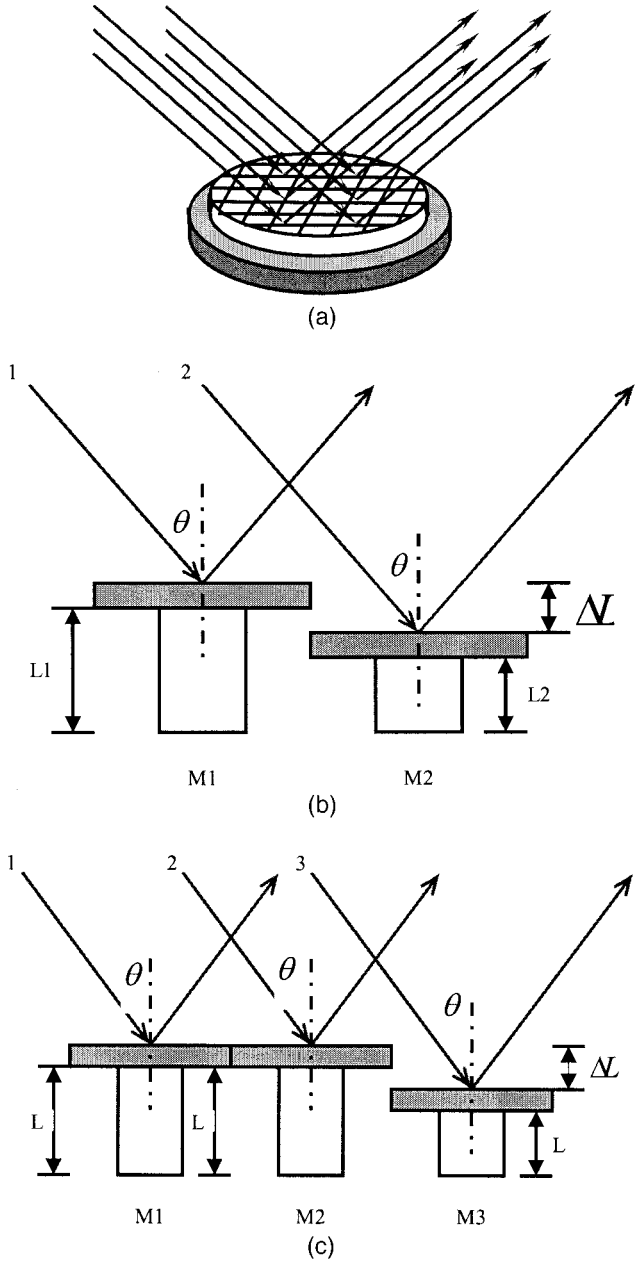

Fig. 4. (a) SDM generated multibeam interference. (b) SDM RTD assignment. (c) SDM RTD magnitude assignment.

According to multibeam interference device design, the RTD spectrum $A(T)$ that can be physically realized is a real and even function. For SDM, all the mirrors should be symmetrically distributed to the zero RTD mirrors as shown in Fig. 5. For $A(T_i)$ with negative value, the mirrors of RTD values of $\pm T_i$ should move an additional distance T_π to realize the negative sign. To keep the mirror distribution symmetric, the mirrors with $+T_i$ RTD should move in the opposite direction to the mirrors with $-L_i$ RTD. The direction could be towards or backwards to the zero RTD mirrors, as shown in Fig. 6.

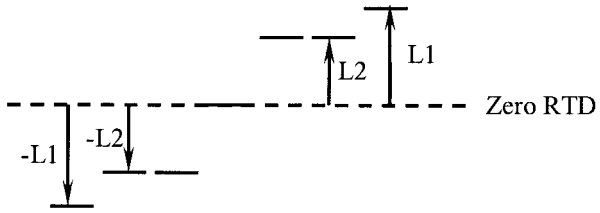

Fig. 5. SDM symmetric distribution.

The proposed SDM adaptive attenuator system for WDM fiber communication is illustrated in Fig. 7. Light from a coherent source S (WDM fiber) is collimated by collimation lens L (W denotes the incident wavefront). The incident light is reflected by the computer controlled SDM (W′ denotes the modulated wavefront). The modulated wavefront is collected by lens L′ and forms multibeam interference on plane P. A fiber is placed at the focal point to collect the light. If the collection is loss-free, then the desired attenuation profile can be realized.

Although the SDM can generate arbitrary interference to some extent, it also has performance limitations. For the SDM, the position of each mirror is controlled by b bits, which would only allow the mirrors to stay at discrete vertical positions with minimum vertical interval of $L/2^b$. Thus for a SDM, its RTD spectrum is discrete and only has nonzero components at multiples of $T = L\cos\theta/c2^{b-1}$. From Fourier-transform theory, a signal that has a discrete frequency spectrum is periodical in the time domain. In analogy, the optical interference spectrum of a SDM is periodical in the optical frequency domain. This periodic structure is a consequence of the mirror vertical position discrete tuning. Let us define this period in the optical frequency domain as the free-spectral range (FSR). Within one FSR, constructive interference occurs at only one wavelength. For all other wavelengths, the beams will be off resonant. Therefore in one FSR, the SDM cannot provide more than one zero-loss peak. This would result in a high insertion loss when compensating an arbitrary spectrum, such as is the case in optical communication. This performance limitation would preclude its uses in applications where low insertion loss is required.

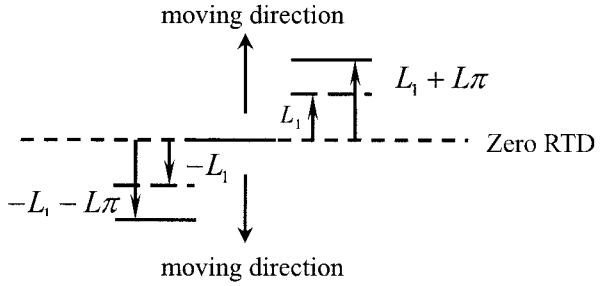

Fig. 6. SDM moving direction.

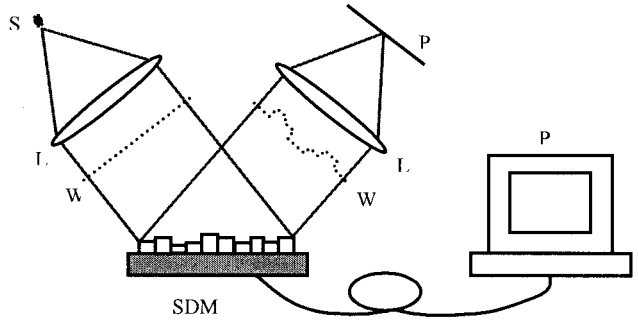

Fig. 7. Idea of the proposed system.

The device performance is simulated. The process of the simulation is illustrated as follows. The real and even RTD spectrum $A(T)$ is first calculated from a given target optical intensity spectrum $I(\omega)$ using Eq. (5) and then Eq. (3). For a SDM with vertical dynamic range L and b-bits control, its vertical position resolution is $L/2^b$, which results in its RTD spectrum resolution of $T = L\cos\theta/c2^{b-1}$. The vertical dynamic range L governs the bandwidth of the SDM. Because $A(T)$ is an even function, the SDM is divided into two groups of mirrors. For each group, the effective vertical dynamic range is $L/2$. Thus for the given SDM, the upper limit of the RTD bandwidth is $T = L\cos\theta/c$. The total number of different RTD components the SDM can provide is 2^{b-1}. Suppose for an $A(T)$, $A'(T)$ is the closest RTD spectrum a SDM can realize. $A'(T)$ is the RTD bandwidth-limited spectrum, and it is unable to provide RTD components in the $A(T)$ that exceed the RTD bandwidth limit of the SDM. $A'(T)$ is also different from $A(T)$ in the normalized magnitudes of each RTD component. Because the negative value $A(T_i)$ is realized by its absolute value $|A(T_i)|$ with an additional vertical shift, $|A(T)|$ is used in normalized RTD magnitude spectrum $A_n(T)$ calculation:

$$A_n(T_i) = \frac{A(T_i)}{\sum |A(T_i)|}. \tag{11}$$

For the normalized magnitude $A_n'(T)$ realized by the SDM, it is equal to the ratio of the number of mirrors in each beam $M(T_i)$ to the total number of mirrors M, such as shown in Equation (12). $M(T_i)$ is derived using Eq. (13). The right side of Eq. (13) is defined as a function to find the closest integer value:

$$A_n'(T_i) = \frac{M(T_i)}{M}, \tag{12}$$

$$M(T_i) = [A_n(T_i) \times M]. \tag{13}$$

Once the normalized RTD spectrum $A_n'(T)$ is obtained, the SDM will assign the $A_n'(T)$ to the beams, and the optical intensity spectrum $I'(\omega)$ is the multibeam interference spectrum of such a device. $I'(\omega)$ is a reproduction of target $I(\omega)$ with distortion. And the purpose of the device design is to minimize this distortion. For a SDM with 3200 mirrors, 10 μm dynamic range, and 10 bit control, light is incident at

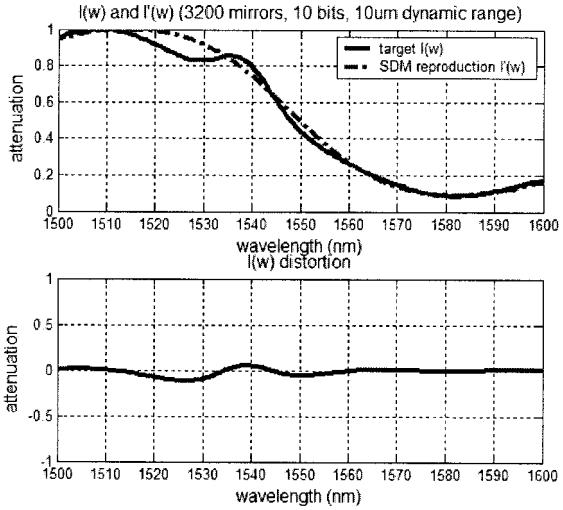

Fig. 8. Comparison of target spectrum and SDM spectrum.

a 15° angle, the RTD resolution is 6.2886×10^{-17} s, the RTD bandwidth is 3.2198×10^{-14} s, and the number of different RTDs is 512. The target $I(\omega)$, the interference spectrum $I'(\omega)$, and the distortion of $I'(\omega)$ from $I(\omega)$ is shown in Fig. 8. The RTD spectrum $A(T)$ obtained from target $I(\omega)$; the RTD spectrum $A_n'(T)$ that is realized by the SDM and their difference is shown in Fig. 9.

In the simulation, the M, L, and b effects on SDM attenuator performance are studied. In the first simulation, the normalized $A(T)$ distortion $A_n(T) - A_n'(T)$, the interference spectra of the three SDMs are compared against each other in Fig. 10. For these SDMs, $L = 10$ μm, $b = 10$, and $M = \{800, 2000, 3200\}$. The result shows that a large number of mirrors leads to less $A(T)$ distortion and better $I'(\omega)$ agreement with $I(\omega)$. In the second simulation, three SDMs are compared, as shown in Fig. 11. The SDMs have $b = 10$, $M = 3200$, and

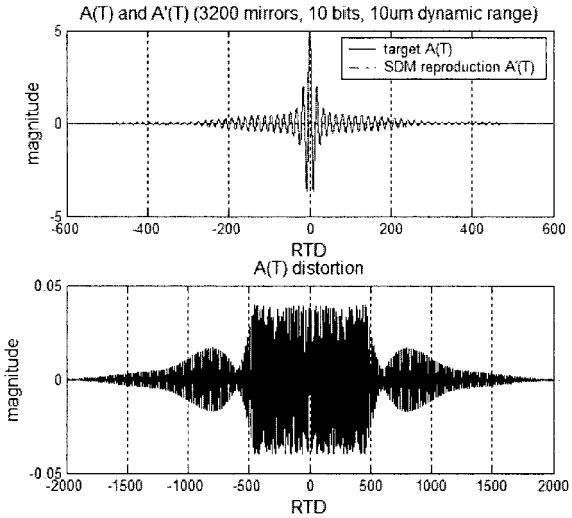

Fig. 9. Comparison of target RTD spectrum and SDM RTD spectrum.

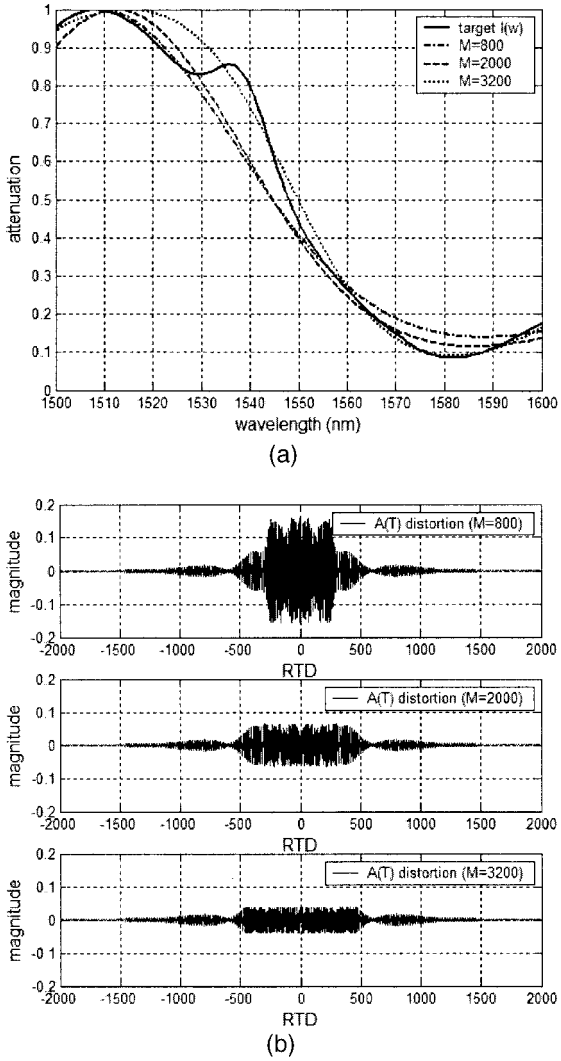

Fig. 10. (a) Spectrum versus mirror number ($L = 10$ μm, $b = 10$). (b) $A(T)$ distortion versus number of mirrors M.

$L = \{4\ \mu\text{m}, 7\ \mu\text{m}, 10\ \mu\text{m}\}$. The result shows that large dynamic range leads to larger RTD bandwidth and a better $I'(\omega)$ agreement with $I(\omega)$. In the third

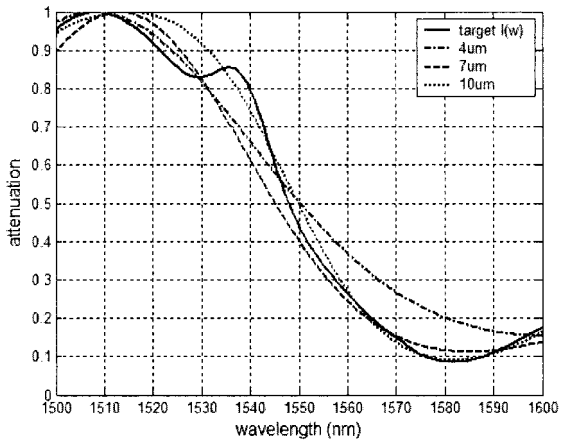

Fig. 11. Spectrum versus dynamic range ($b = 10, M = 3200$).

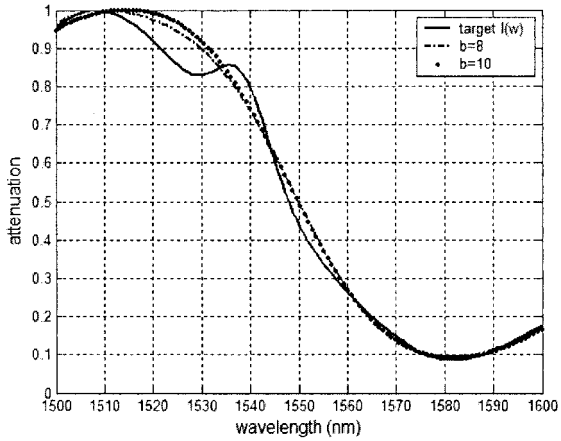

Fig. 12. Spectrum versus number of bits ($L = 10\ \mu m, M = 3200$).

simulation, two SDMs that have $L = 10\ \mu m$, $M = 3200$, and $b = \{8, 10\}$ are compared, as shown in Fig. 12. The b together with L determines at which interval the RTD spectrum $A(T)$ is sampled. Larger b leads to a smaller interval and more RTD components within a fixed RTD bandwidth, which in turn gives less $I(\omega)$ distortion. As a general rule, the larger the M, L, and b values, the better the agreement between $I'(\omega)$ and $I(\omega)$.

5. Summary

Fourier analysis is a powerful tool in multibeam interference analysis and design. By using such full-developed approach, optical attenuators can be designed in a similar way as time-domain signal filters. The general principle of optical attenuator design is given. The novel adaptive attenuator has an optimum structure due to the general principle. Its advantages are real-time arbitrary spectrum shaping, low insertion loss, high-speed tunability, simple device structure, and high flexibility.

References

1. C. R. Doerr, P. Schiffer, L. W. Stulz, M. Cappuzzo, E. Laskowski, A. Paunescu, L. Gomez, and J. Gates, "Compact integrated dynamic wavelength equalizer," in *Optical Fiber Communication Conference, 1999 OSA Technical Digest Series* (Optical Society of America, Washington, D.C., 1999), paper PD30 Suppl.
2. N. A. Riza, "Fault-tolerant fiber-optical beam control modules," U.S. patent 6,222,954 (24 April 2001).
3. A. Vladimir, B. Bradley, D. Bishop, G. Clinton, S. Lawrence, and R. Rene, "Optical attenuator," U.S. patent 6,173,105 (9 January 2001).
4. E. E. Bergmann and D. Bishop, "Micro-mechanical variable optical attenuator," U.S. patent 6,163,643 (19 December 2000).
5. R. R. Abbott, G. W. Berkstresser, C. D. Brandle, Jr., V. J. Fratello, and S. J. Licht, "Article comprising a variable optical attenuator," U.S. patent 5,978,135 (2 November 1999).
6. S. H. Huang, X. Y. Zhou, S. M. Hwang, A. E. Willner, Z. Bao, and D. A. Smith, "Experimental demonstration of dynamic network equalization of three 2.5 Gb/s WDM channels over 1000 km using acoustooptic tunable filters," IEEE Photonics Technol. Lett. **8,** 1243–1245 (1996).
7. H. S. Kim, S. H. Yun, H. K. Kim, N. Park, and B. Y. Kim, "Actively gain-flattened erbium-doped fiber amplifier over 35 nm by using all-fiber acoustooptic tunable filters," IEEE Photonics Technol. Lett. **10,** 790–792 (1998).
8. K. Inoue, T. Kominato, and H. Toba, "Tunable gain equalization using a Mach–Zehnder optical filter in multistage fiber amplifiers," IEEE Photonics Technol. Lett. **3,** 718–720 (1991).
9. M. Zirngibl, C. H. Joyner, and B. Glance, "Digitally tunable channel dropping filter/equalizer based on waveguide grating router and optical amplifier integration," IEEE Photonics Technol. Lett. **6,** 513–515 (1994).
10. C. R. Doerr, C. H. Joyner, and L. W. Stulz, "Integrated WDM dynamic power equalizer with potentially low insertion loss," IEEE Photonics Technol. Lett. **10,** 1443–1445 (1998).
11. M. C. Parker, A. D. Cohen, and R. J. Mears, "Dynamic holographic spectral equalization for WDM," IEEE Photonics Technol. Lett. **9,** 529–531 (1997).